Hindawi
Adsorption Science & Technology
Volume 2023, Article ID 7581943, 13 pages
https://doi.org/10.1155/2023/7581943

Research Article

Silicon Dioxide Functionalized with Oxygen–Containing Groups for Enhanced BCl_3 Adsorption

Miaolei Zhang, Jianhua Liu, and Guoqiang Huang

School of Chemical Engineering and Technology, Tianjin University, Tianjin 300350, China

Correspondence should be addressed to Guoqiang Huang; hgq@tju.edu.cn

Received 9 January 2023; Revised 24 March 2023; Accepted 29 March 2023; Published 15 April 2023

Academic Editor: Muhammad Raziq Rahimi Kooh

Copyright © 2023 Miaolei Zhang et al. This is an open access article distributed under the Creative Commons Attribution License, which permits unrestricted use, distribution, and reproduction in any medium, provided the original work is properly cited.

Boron chloride in the chlorosilane is hard to remove and directly impacts the quality of polysilicon produced by improved Siemens method. Silicon dioxide functionalized with mannitol and citric acid successfully removed boron chloride in organic solution. The effects of immersion concentration and drying temperature were studied to attain the best adsorption performance. The sorption phenomenon was described well by pseudo-second-order kinetic model and Langmuir adsorption isotherm; particle diffusion model proved that the adsorption on the active adsorption site was the rate determining step, with the formation of boronic esters. Thermal stability and degradation kinetic of the adsorbents were investigated by thermogravimetric analysis. The characterization results of Fourier transform infrared spectroscopy, thermogravimetric analysis, X-ray energy spectrometry, and BET showed the silicon dioxide was successfully functionalized by oxygen-containing functional groups, leading to be a better and safer substitute to traditional boron-selective chelating resin.

1. Introduction

In the face of an energy crisis and environmental degradation and growing demand for low carbon emission reduction, the unlimited, nonpolluting, and extremely abundant solar power is seen as an effective decarbonization scenario [1], and the market of photovoltaic technology is rapidly evolving with a compound annual growth rate (CAGR) equal to 34% between 2010 and 2020 [2]. Silicon-based solar cells account for more than 94% of the PV market due to the low cost, high photoelectric conversion efficiency, and stability [3]. The quality of polysilicon products greatly affects the photoelectric conversion efficiency and stability.

At present, improved Siemens method [4] is the main production process of polysilicon. Trichlorosilane is prepared by hydrogenation of silicon tetrachloride, and then trichlorosilane is reduced by hydrogen and deposited on the silicon core heater to produce the polysilicon. As the typical acceptor impurity, the trace boron impurities in the raw material of trichlorosilane directly affect the quality and conduction type of polysilicon products. The tolerance limit of boron impurity in solar-grade polycrystalline silicon required by China [5] is below 0.1×10^{-9}, and boron impurity in electronic-grade polycrystalline silicon [6] is required to be less than 5×10^{-11}. The trace boron compounds are complex in the trichlorosilane. Conventional wisdom holds that the main boron compound impurities are BCl_3, B_2Cl_6, or other complex forms. The boiling point of these impurities is too close to chlorosilane to be separated by multistage distillation [7]. The purification methods [8] of boron impurity from chlorosilane include extraction, complexation, adsorption, and partial hydrolysis [9, 10]. Some of these techniques are effective but have some limitation. The partial hydrolysis tends to lead to strong silicification of the device and generate large amounts of corrosive hydrogen chloride [11, 12]. The extraction method [13, 14] is highly efficient, but overall, a lot of work is still needed to find a suitable complexing agent, and there is a lack of in-depth research on the complexing process and mechanism in the actual industrial production.

Compared with other methods, the adsorption method is currently the most widely used in the industry, and the commonly used adsorption material includes activated

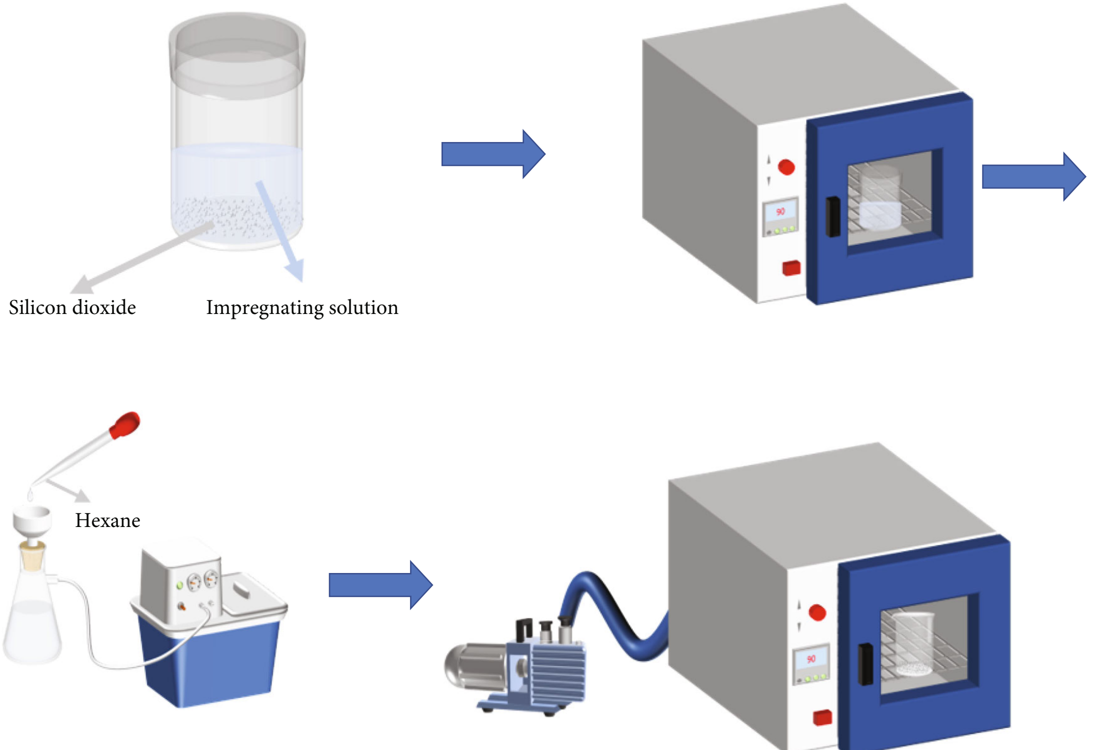

Figure 1: Schematic illustration of the process of silicon dioxide impregnation.

carbon [15], ion-exchange resin [16, 17], or boron-selective chelating resin (e.g., Amberlite RA-743, Dowex BSA-1, and D564) [18, 19], which has a macroporous polystyrene backbone to which the functional group (glucosamine) is attached. Glucosamine can bond covalently to boron impurities, resulting an excellent boron removal performance. However, the chlorosilane is flammable and explosive. The large amount of flammable chelating resin will pose a huge hidden hazard in case of leakage accidents, resulting in the need for the safe and cheap boron adsorption agent.

The boron impurities like BCl_3 in chlorosilane exhibit similar electron deficiency to the H_3BO_3 in aqueous solution, which has been well studied, and some mentioned commercial boron-selective chelating resin has been developed and widely used in seawater desalination, boron halogenation, and other fields [19]. Further researches focus on material with higher selectivity and easier separation, and Oladipo and Gazi [20, 21] developed hydroxyl-enhanced magnetic material that performed better and can be easily separated from the suspensions by an external magnet, leading to be a techno-economic substitute to the existing boron adsorbents [22]. It is concluded that most reported boron adsorbents for H_3BO_3 in aqueous solution have electron-rich group that plays a key role in the boron removal, leading to the electron-rich oxygen-containing inorganic adsorbent for BCl_3 in this study.

As the inorganic and nonflammable material, the surface of silicon dioxide is covered with the large number of electron-rich hydroxyl groups [23], so it was applied in the removal of boron impurities [24]. Besides, it possesses the advantages of being easily modified, the stable physical and chemical properties, good mechanical strength, high specific surface area, and pore capacity [25].

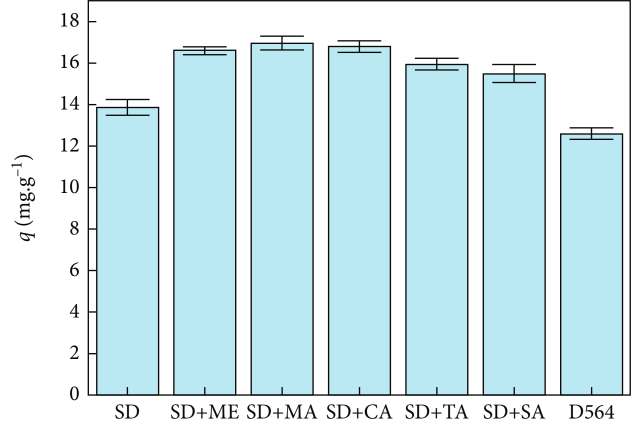

Figure 2: Comparison of boron adsorption capacity on SD, SD + ME, SD + MA, SD + CA, SD + TA, SD + SA, and D564.

The study is aimed at investigating boron chloride adsorption on silicon dioxide impregnated with different functional groups and attaining better removal performance, which was evaluated using equilibrium, kinetic, and thermodynamic studies.

2. Materials and Methods

2.1. Reagent and Instrument. All chemicals, silicon dioxide (CP, purchased from Tianjin Guangfu Technology Development Co., Ltd.), boron chloride in hexane (CP, provided by

Figure 3: Structure of impregnating agent (ME, MA, CA, TA, and SA).

Aladding), methylamine-H, L-ascorbic acid, ammonium acetate, acetic acid, disodium EDTA dihydrate, tartaric acid, (CP, provided by Macklin), meglumine, mannitol, citric acid, salicylic acid (CP, bought from Heowns), and boron-selective chelating resin (D564) (provided by Shanghai Yuanye Bio-Technology Co., Ltd.), were directly used and without further purification.

Ultrasonic cleaner (SK7200B), Shanghai KD Ultrasonic Instrument Co., Ltd; UV-Visible spectropho-tometer (754 N), Shanghai Yidian Analytical Instrument Co., Ltd.

Fourier transform infrared (FT-IR) spectrum was collected on a Thermo Fisher Nicolet iZ10 using KBr as standard reference in the range of 400–4000 cm^{-1}. The thermogravimetric analyses (TGA) were performed on a NETZSCH 209F3 derivatograph. The data recording occurred in 250 ml•min^{-1} outflow air, within the 30–950°C temperature range and at the 20 K•min^{-1} rates of heating. The specific surface area was tested and calculated by Micromeritics.

2.2. Silicon Dioxide Impregnation. The process of impregnation was described in Figure 1, and about 5 g of silicon dioxide was impregnated in the 100 cm^3 impregnating solution (weight concentration range of 0.2–3%) for 12 h at 90°C. The impregnated silicon dioxide was collected by filtration, washed by hexane, and vacuum dried at 70, 90, 110, 130, 150, and 170°C to constant weight. The impregnating substance used was meglumine (ME), mannitol (MA), citric acid (CA), tartaric acid (TA), and salicylic acid (SA).

2.3. Static Adsorption. Due to the flammable and explosive property of chlorosilane, the boron chloride in chlorosilane was replaced by the boron chloride in hexane in the study. The tests were carried in the screw capped bottles with polyethylene gaskets filled with N_2, which prevents the boron chloride from water steam.

During static experiments, adsorbent (0.1, 0.2, or 0.5 g) was put into the 15 or 30 ml hexane solution of boron chloride at the concentration of 585 ppm at room temperature for 2 h.

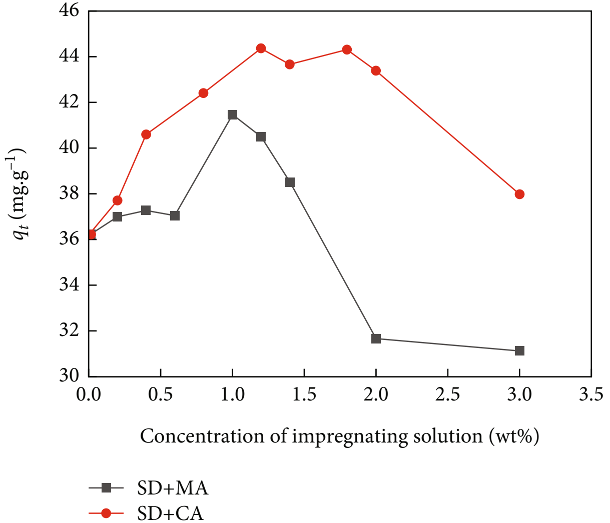

Figure 4: The effect of concentration of impregnating solution on boron adsorption capacity on SD + MA and SD + CA.

In kinetic experiments, the boron concentration was measured by sampling at regular intervals until the concentration remained constant, which means the adsorption equilibrium reached.

In order to investigate the dependence on the initial boron concentration, the concentration of the solution varied between 234 ppm and 23400 ppm, while the 0.1 g of adsorbents was weighted into the 15 ml of the hexane solution of boron chloride.

The adsorption capacity (q) of boron chloride is given as

$$q = \frac{(c_0 - c) \times V}{m} \quad (1)$$

Table 1: The pore size of different adsorbents impregnated by solution of different concentration.

Adsorbents	Concentration of impregnating solution W%	Surface area ($m^2 \cdot g^{-1}$)	Pore volume ($cm^3 \cdot g^{-1}$)	Pore size (A)
SD	\	307	0.9994	130.2
SD + MA	1.0	234	0.9611	164.0
SD + MA	3.0	287	0.9209	128.2
SD + CA	1.0	287	0.9599	133.7
SD + CA	3.0	266	0.8376	126.1

where c_0 and c are the initial and residual boron chloride concentration in the solution, mg•l^{-1}; V is the volume of boron chloride solution, l; m is the amount of adsorbents added in the solution, g.

Boron chloride in hexane was hydrolysed to form boric acid solution [26], then it was measured spectrophotometrically using azomethine-H, which will form yellow complex with boric acid after 6 h of waiting time, and then the absorbance value was tested at 415 nm, with a 1 cm cuvette against the blank test [27].

3. Results and Discussion

3.1. Static Adsorption Experiments of Adsorbent. As polyols and organic acids have typical oxygen–containing functional groups that definitely enhance the boron adsorption as reported [28, 29], the adsorption ability of boron chloride on impregnated silicon dioxide showed different increase with different impregnating agent in Figure 2. The result points to silicon dioxide impregnated with mannitol (SD + MA) and citric acid (SD + CA) as the best adsorbents of boron chloride in this study, which can be attributed to the structure and number of oxygen-containing functional groups. The structure of impregnating agent is shown in Figure 3, MA and ME are both polyols, and MA has more hydroxy than ME, resulting little better performance than ME. Compared with CA and TA, SA has less hydroxy and carboxy, leading to a lower adsorption capacity.

3.2. The Effect of Impregnating Concentration. Figure 4 presents the adsorption capacity of boron chloride on impregnated silicon dioxide prepared with different impregnating solution concentration, and the adsorption capacity of boron chloride on impregnated silicon dioxide increased at early stage and then decreased with increasing impregnating solution concentration. The maximum adsorption capacity of SD + CA is 44.37 mg•g^{-1}at 1.2% of impregnating solution, and the maximum adsorption capacity of SD + MA is 40.49 mg•g^{-1} at 1% of impregnating solution, which is attributed to the increasing loading of the oxygen-containing active sites on the surface of silicon dioxide with the increasing concentration of impregnating solution. However, with further increase in concentration, as shown in Table 1, some functional groups may agglomerate and block the limited loading sites of silicon dioxide, resulting in the decrease in the pore size, pore volume, and decrease in adsorption capacity of impregnated silicon dioxide. When the concentration of mannitol impregnation solution reached 3%, the pore channels may be blocked or even disappeared, the

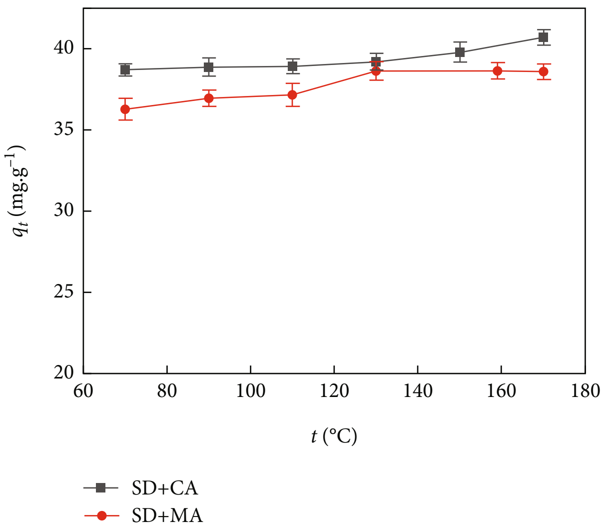

Figure 5: The effect of drying temperature on boron adsorption capacity on SD + MA and SD + CA.

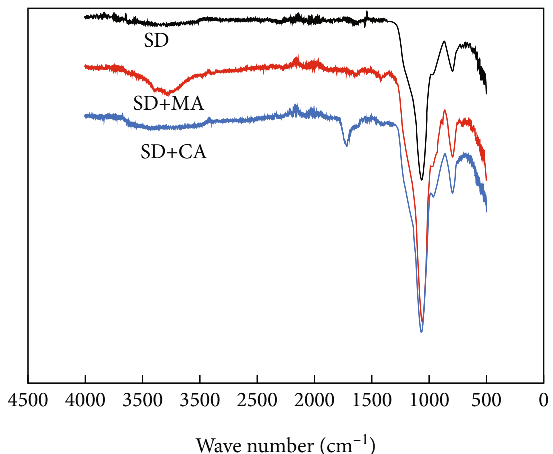

Figure 6: FT-IR spectra of SD, SD + MA, and SD + CA.

Table 2: The relative percentage of C, O, and Si in adsorbents determined by EDS.

Adsorbents	Concentration of impregnating solution W%	C%	O%	Si%
SD + MA	1.0	15.75	61.25	22.99
SD + CA	1.0	13.35	56.26	30.39

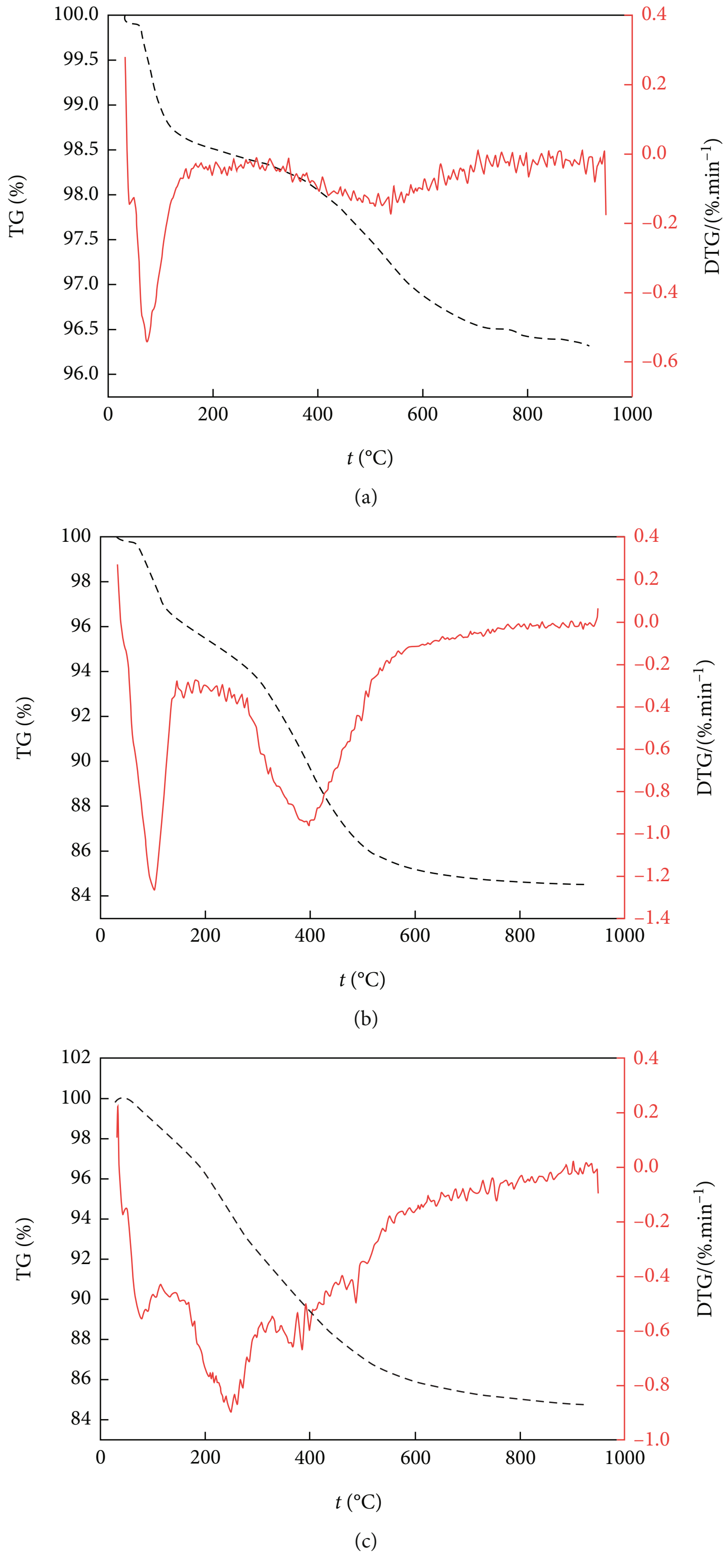

Figure 7: TGA and DTG curves for (a) SD, (b) SD + MA, and (c) SD + CA.

internal diffusion of boron chloride mainly control the adsorption, and boron chloride cannot enter the pore channels of impregnated silicon dioxide, which caused the adsorption capacity of SD + MA to drop sharply, even lower than that of blank silicon dioxide.

3.3. The Effect of Drying Temperature. As can be shown in Figure 5, with the increase of the drying temperature, little change in adsorption capacity indicates that the drying temperature had little effect on the increase of active oxygen-containing group sites. But the increasing temperature may

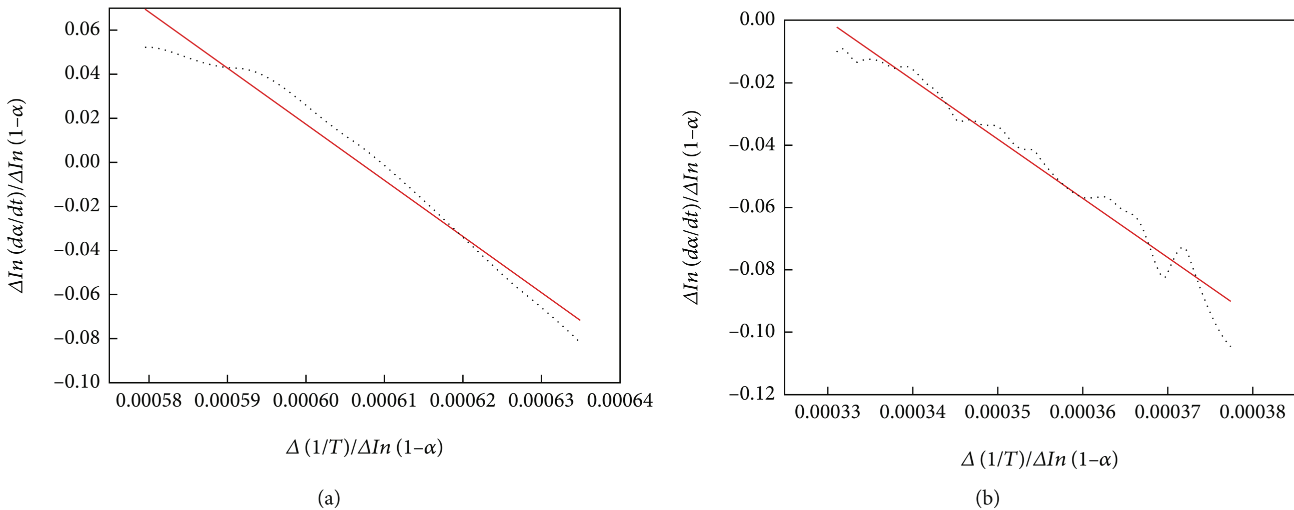

Figure 8: Thermal degradation kinetic curves of (a) SD + MA in 69.6–103.1°C and (b) SD + MA in 311.7–397.4°C.

promote the bonding of mannitol to the hydroxyl groups on the surface of silicon dioxide.

3.4. Characterization. Functional groups identified by FT-IR spectra in Figure 6 confirm the successful functionalization of mannitol and citric acid on the surface of silicon dioxide, and the FT-IR spectra of impregnated adsorbents show the increase in the band at 3400 cm^{-1} (ν-OH) [30] and the appearance of new peak at 2904 cm^{-1} and 2844 cm^{-1} (ν-CH) [31], suggesting the successful grafting of polyol groups on the silicon dioxide supports. The appearance of a new peak at 1760 cm^{-1} (ν-C=O) and 1410 cm^{-1} (δ-C-OH) [30] and the wide and scattered peak at the range of 3200 cm^{-1}–2500 cm^{-1} [30] suggest the loading of carboxylic acid on the silicon dioxide.

Active silicon dioxide and impregnated silicon dioxide were analyzed by X-ray energy spectrometry (EDS). It was found in Table 2 that the proportion of elemental Si on the surface of the impregnated silicon dioxide decreased, and the content of elemental C increased significantly compared to the activated silicon dioxide, which was attributed to the loading of polyhydroxy organic compounds on the surface of silicon dioxide.

Figure 7 shows the TGA curves of the studied adsorbents from ambient temperature to 950°C at heating rates of 20°C•min^{-1}. In these curves, the mass loss of all adsorbents started at about 95°C and ended around 500°C. The mass residue was mainly SiO_2, the product of inorganic silicon combustion, and the thermal decomposition of analyzed polymers occurred in two or three well-defined stages.

Thus, in the case of silicon dioxide, the first stage began at about 40°C and ended at about 97.5°C, characterized by weak DTG peak at 74.8°C, which can be mainly attributed to the adsorbed water. This stage involved maximum 0.98% weight loss and can be considered nondegradable. The second stage, which began at around 360°C and ended at about 630°C, can be attributed to the decomposition of hydroxyl groups on the surface of silicon dioxide.

The SD + MA exhibits two distinct stages of decomposition. Thus, the first stage began at 69.6°C and ended at about

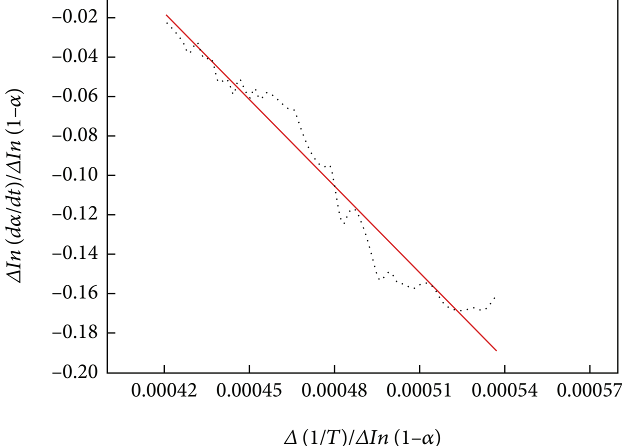

Figure 9: Thermal degradation kinetic curves of SD + CA in 92.8–249.6°C.

122°C, with DTG peak at about 103.1°C, which can be mainly attributed to the residual solvent, and this step involved 4.23% mass loss. The second stage started at around 311.7°C and ended at around 494.5°C with DTG peaking at 397.4°C, mainly due to the thermal decomposition of mannitol, which involved 11.25% mass loss.

The steady mass loss in SD + CA started at about 92.8°C, ended at 950°C, and was characterized by a DTG peak of 249.6°C, which was due to the mass loss of the citric acid on the silicon dioxide, and the weight loss rate was 15.17%. The difference between silicon dioxide and impregnated adsorbents shows that mannitol and citric acid are indeed loaded onto the surface of the silicon dioxide.

3.5. Thermal Degradation Kinetic of Adsorbents. In order to explain the thermal degradation of synthesized adsorbents, it is necessary to know the whole kinetic triplet [32, 33]. At each stage of the beginning and end of decomposition, kinetic analysis was performed using Freeman-Carroll method [34] to calculate the activating energy, pre-

Table 3: Kinetic properties for adsorbents using Freeman-Carroll method.

Adsorbents	SD + MA			SD + AC		
Parameter	E (KJ•mol^{-1})	n	R^2	E (KJ•mol^{-1})	n	R^2
Stage I	21.14	1.543	0.9691	12.17	0.5974	0.9602
Stage II	15.74	0.6244	0.9694			

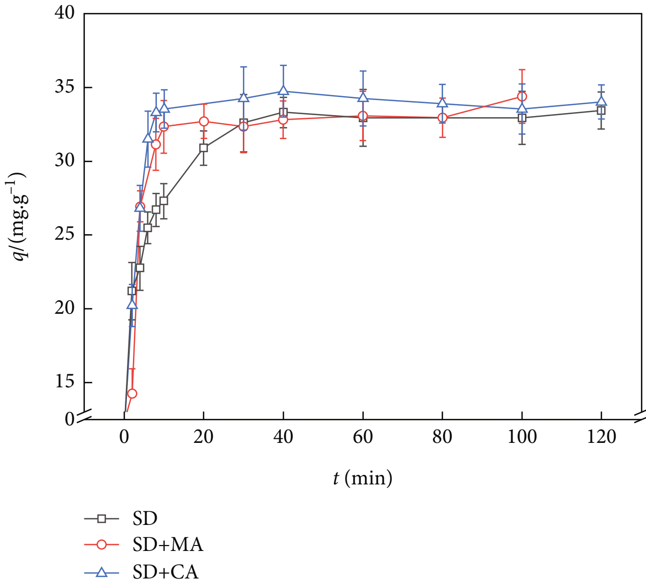

Figure 10: Effect of reaction time on removal of boron chloride on SD, SD + MA, and SD + CA.

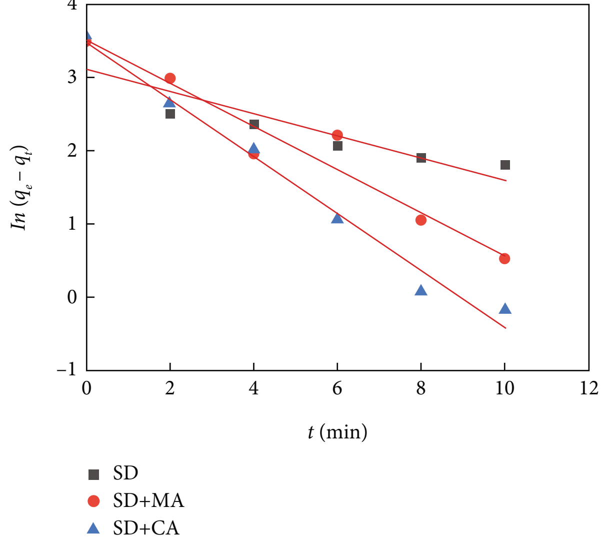

Figure 11: The pseudo-first-order kinetic model fitting of adsorption kinetics curves of SD, SD + MA, and SD + CA.

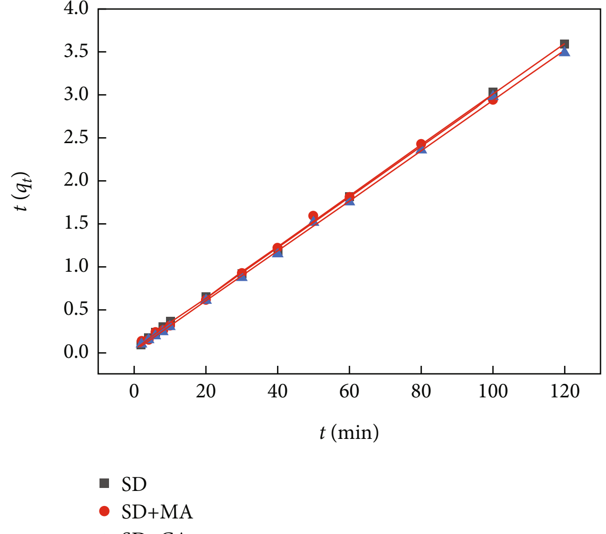

Figure 12: The pseudo-second-order kinetic model fitting of adsorption kinetics curves of SD, SD + MA, and SD + CA.

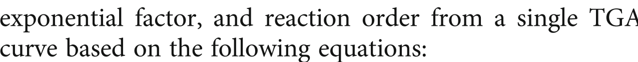

exponential factor, and reaction order from a single TGA curve based on the following equations:

$$\frac{d\alpha}{dt} = Ae^{-E/\mathrm{RT}}(1-\alpha)^n \quad (2)$$

or

$$\frac{\Delta \mathrm{In}(d\alpha/dt)}{\Delta \mathrm{In}(1-\alpha)} = -\frac{E}{R}\frac{\Delta(1/T)}{\Delta \mathrm{In}(1-\alpha)} + n \quad (3)$$

TABLE 4: Kinetic parameters of adsorption of boron chloride on SD, SD + MA, and SD + CA.

Adsorbents	t_e (min)	q_e (exp) (mg·g^{-1})	Pseudo-first-order kinetic model				Pseudo-second-order kinetic model			
			q_e (fit) (mg·g^{-1})	k_1 (min^{-1})	χ	R^2	q_e (fit) (mg·g^{-1})	k_2 (g.mg^{-1} min^{-1})	χ	R^2
SD	40	33.42	22.59	0.1512	0.4794	0.8279	33.81	1.725×10^{-2}	1.153×10^{-2}	0.9998
SD + MA	10	34.02	33.52	0.2939	0.01493	0.9417	34.00	1.817×10^{-2}	5.882×10^{-4}	0.9987
SD + CA	10	34.38	32.28	0.3892	0.06506	0.9848	34.26	4.691×10^{-2}	3.503×10^{-3}	0.9996

Note: q_e(exp) and q_e(fit) are the equilibrium experiment results and calculated value according the model, respectively.

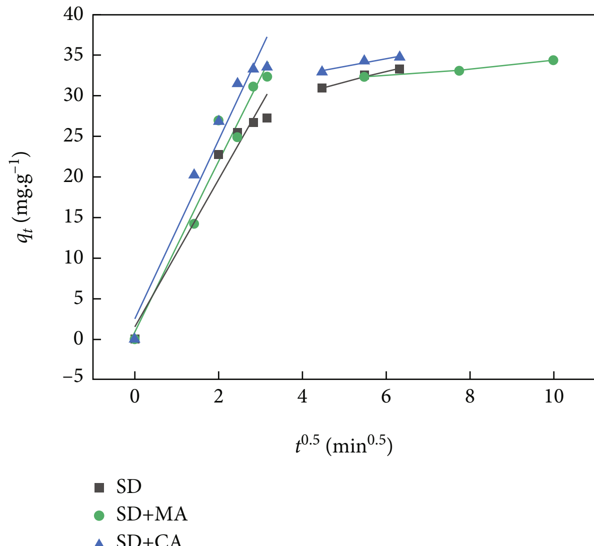

FIGURE 13: Multisegment fitting curve of the intraparticle diffusion model of adsorption of boron chloride on SD, SD + MA, and SD + CA.

TABLE 5: Diffusion parameters in particles of adsorption of boron chloride on SD, SD + MA, and SD + CA.

Adsorbents	Section I			Section II		
	k_n	C	R^2	k_n	C	R^2
SD	9.082	1.485	0.9560	1.307	25.17	0.9687
SD + MA	10.55	0.7507	0.9545	0.4509	29.77	0.9714
SD + CA	11.01	2.484	0.9479	0.9822	28.65	0.9549

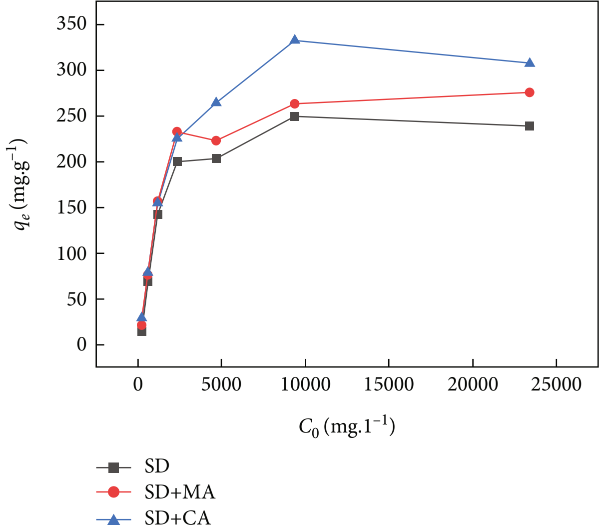

FIGURE 14: Adsorption isotherms of removal of boron chloride on SD, SD + MA, and SD + CA.

where $d\alpha/dt$ is the rate of reaction, s^{-1}, α is the conversion of reaction, n is the order of reaction, R is the gas constant, 8.31 J•mol^{-1}•K^{-1}, T is the degradation temperature, K, A is the pre-exponential factor, and E is the apparent activation energy in J•mol^{-1}.

The results of the thermal degradation kinetic were shown in Figures 8 and 9.

The kinetic parameters corresponding to the degradation of impregnated adsorbents are presented in Table 3.

As can be seen from the data in Table 3 that the activation energy and the order of reaction are not always a constant value, proving that the thermal degradation of mannitol-modified silica is a complex reaction.

3.6. Adsorption Kinetics Experiments of Adsorbents. Adsorption equilibrium curves described in Figure 10 show that the adsorption rate of boron chloride in solution is fast. The adsorption capacity increased rapidly with the increase of adsorption time in the first 10 minutes, after which, it slowed down as the adsorption equilibrium was reached. This is a typical development rule in adsorption process. As the adsorption progresses, the diffusion rate of solute to adsorbent slows due to the decrease of adsorption concentration [35]. The experimental results obtained were used to study the rate-limiting step.

The adsorption kinetics curves were analyzed using the pseudo-first-order kinetic equation as follows [30]:

$$\ln (q_e - q_t) = \ln q_e - k_1 t \quad (4)$$

The pseudo-second-order adsorption kinetic equation can be expressed as follows [36]:

$$\frac{t}{q_t} = \frac{1}{k_2 q_e^2} + \frac{t}{q_e} \quad (5)$$

where q_e and q_t are the adsorption capacity, mg•g^{-1}, at equilibrium and at time t, respectively, t is the adsorption time, min, k_1 is the pseudo-first-order adsorption rate constant, min^{-1}, and k_2 is the pseudosecondary adsorption rate constant, g•mg^{-1}•min^{-1}.

Table 6: Two parameters adsorption isotherm parameters of boron chloride on SD, SD + MA, and SD + CA.

Adsorbents	q_e(exp) (mg·g^{-1})	Isotherms and parameters			
		Langmuir	Freundlich	Temkin	Dubinin-Radushkevich
SD	249.6	$q_l = 250.0$	$K_f = 82.42$	$B = 30.78$	$q_D = 226.0$
		$k_l = 1.471 \times 10^{-3}$	$1/n_f = 0.1152$	$A = -43.00$	$A_D = 2.843 \times 10^4$
		$\Delta q_t = 0.4000$	$\Delta q_t = 10.46$	$\Delta q_t = 14.95$	$\Delta q_t = 23.54$
		$\chi = 1.600 \times 10^{-3}$	$\chi = 4.021 \times 10^{-2}$	$\chi = 5.652 \times 10^{-2}$	$\chi = 0.1041$
		$R^2 = 0.9898$	$R^2 = 0.8573$	$R^2 = 0.8429$	$R^2 = 0.9088$
SD + MA	275.8	$q_l = 277.8$	$K_f = 103.3$	$B = 30.42$	$q_D = 250.8$
		$k_l = 2.091 \times 10^{-3}$	$1/n_f = 0.1024$	$A = -12.29$	$A_D = 1.012 \times 10^4$
		$\Delta q_t = 2.000$	$\Delta q_t = 10.00$	$\Delta q_t = 15.47$	$\Delta q_t = 25.00$
		$\chi = 7.199 \times 10^{-3}$	$\chi = 3.503 \times 10^{-2}$	$\chi = 5.313 \times 10^{-2}$	$\chi = 9.968 \times 10^{-2}$
		$R^2 = 0.9977$	$R^2 = 0.8619$	$R^2 = 0.8419$	$R^2 = 0.8863$
SD + CA	332.6	$q_l = 312.5$	$K_f = 43.65$	$B = 45.32$	$q_D = 276.7$
		$k_l = 4.555 \times 10^{-3}$	$1/n_f = 0.2176$	$A = -100.5$	$A_D = 6.181 \times 10^3$
		$\Delta q_t = 20.05$	$\Delta q_t = 50.96$	$\Delta q_t = 18.73$	$\Delta q_t = 55.91$
		$\chi = 6.416 \times 10^{-2}$	$\chi = 0.1329$	$\chi = 5.327 \times 10^{-2}$	$\chi = 0.2021$
		$R^2 = 0.9981$	$R^2 = 0.8492$	$R^2 = 0.9262$	$R^2 = 0.8761$

Table 7: Three parameters adsorption isotherm parameters of boron chloride on SD, SD + MA, and SD + CA.

Adsorbents		Redlich-Peterson	Sips	Toth
SD	$q_e(\text{exp}) = 249.5$	$A_{RP} = 0.6920$	$q_s = 223.4$	$q_T = 232.6$
		$B_{RP} = 2.261 \times 10^{-3}$	$K_s = 5.149 \times 10^{-3}$	$K_t = 2.272 \times 10^{-3}$
		$g = 1.024$	$n_s = 0.2572$	$t = 1.707$
		$\Delta q_t = 12.42$	$\Delta q_t = 26.11$	$\Delta q_t = 16.99$
		$\chi = 0.05218$	$\chi = 0.1169$	$\chi = 0.07308$
		$R^2 = 0.8703$	$R^2 = 0.9116$	$R^2 = 0.8777$
SD + MA	$q_e(\text{exp}) = 275.8$	$A_{RP} = 1.417$	$q_s = 249.2$	$q_T = 247.5$
		$B_{RP} = 5.573 \times 10^{-3}$	$K_s = 8.713 \times 10^{-3}$	$K_t = 3.593 \times 10^{-3}$
		$g = 0.9944$	$n_s = 0.2165$	$t = 134.0$
		$\Delta q_t = 8.062$	$\Delta q_t = 26.62$	$\Delta q_t = 28.32$
		$\chi = 0.03011$	$\chi = 0.1068$	$\chi = 0.1144$
		$R^2 = 0.8555$	$R^2 = 0.8969$	$R^2 = 0.8632$
SD + CA	$q_e(\text{exp}) = 332.6$	$A_{RP} = 1.879$	$q_s = 321.0$	$q_T = 326.4$
		$B_{RP} = 8.993 \times 10^{-2}3$	$K_s = 4.211 \times 10^{-3}$	$K_t = 7.041 \times 10^{-3}$
		$g = 0.9565$	$n_s = 1.197$	$t = 0.7387$
		$\Delta q_t = 14.24$	$\Delta q_t = 11.60$	$\Delta q_t = 6.183$
		$\chi = 0.04514$	$\chi = 0.03613$	$\chi = 0.01892$
		$R^2 = 0.9611$	$R^2 = 0.9575$	$R^2 = 0.9596$

The correlation coefficients and the rate constants for the pseudo-first-order kinetic model and pseudo-second-order kinetic model are shown in Figure 11, Figure 12, and Table 4, respectively.

R^2 and χ can be used to assess how well the kinetic model coincides with the experiment data, $\chi = |q_e(\text{exp}) - q_e(\text{fit})|/q_e(\text{fit})$; if the experimental results are similar to the data from the model, χ will be small else it will be large

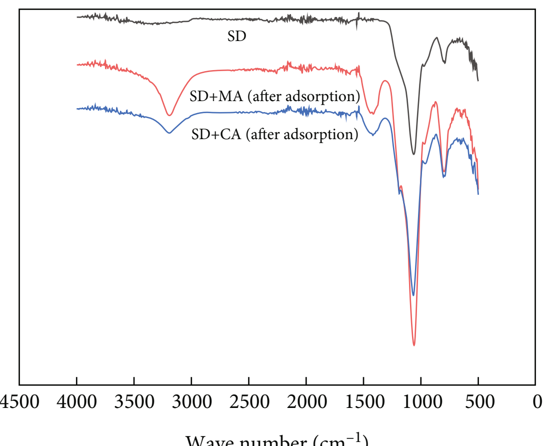

FIGURE 15: FT-IR spectra of SD, SD + MA after adsorption, and SD + CA after adsorption.

[29]. Larger R^2 and smaller χ obtained from the pseudo-second-order kinetic model indicate that the adsorption of boron chloride on silicon dioxide can be described by the second-order kinetic reaction model better. It can be concluded that the adsorption rate is mainly controlled by chemisorption.

The control steps of the speed of adsorption process are usually investigated using the diffusion model in the particle [37], and the formula is as follows:

$$q_t = k_n t^{1/2} + C \tag{6}$$

where q_t is the adsorption capacity of adsorbents on boron chloride at a certain time, mg•g^{-1}, t is the adsorption time, min, k_n is the diffusion rate constant in the particle, and C is a constant.

Typically, the particle diffusion model is three-stage linear, including boundary layer diffusion, internal diffusion, and adsorption site adsorption. Because the first stage reaction speed is very fast, it will not be the control step of adsorption reaction, so the adsorption data were fitted in two stages and shown in Figure 13.

As can be seen from the Table 5, the R^2 of two stages is greater than 0.9, and the fit lines do not pass through the point of origin, indicating that the adsorption process is a complex process mixed with physical adsorption and chemical adsorption. The diffusion coefficient k_n of section II is smaller than that of section I, which proves that the adsorption of boron chloride is controlled by the adsorption on the active adsorption site.

3.7. Determination of Adsorption Isotherm. The distribution of boron between the liquid phase and the solid phase is an index of equilibrium position during the adsorption.

Adsorption isotherm was shown in Figure 14, silicon oxide adsorption of boron chloride can be roughly divided into several stages at concentrations of boron chloride ranging from 234 ppm to 2340 ppm, the adsorption capacity increased with the increase of the concentration of boron chloride solution, the increasing trend slowed down within 2340 ppm to 9360 ppm, and the adsorption capacity basically remained unchanged within 9360 ppm to 23400 ppm.

The adsorption isotherms were analyzed by two-parameter models: Langmuir, Freundlich, Temkin, and Dubinin-Radushkevich and three-parameter models: Redlich-Peterson, Sips, Toth, etc. [38].

Langmuir equation assumes that the maximum adsorption occurs when the surface is covered by a monolayer of adsorbate, which is effective for monolayer sorption onto a surface with a finite number of identical sites [36], as shown below:

$$q_e = \frac{k_l q_l c_e}{1 + k_l c_e}, \tag{7}$$

where q_e is the adsorption capacity at adsorption equilibrium, mg•g^{-1}, c_e is the concentration of boron chloride at adsorption equilibrium, mg•l^{-1}, q_l is the maximum theoretical monolayer adsorption capacity, mg•g^{-1}, and k_l is the adsorption equilibrium constant, which is related to the enthalpy change of adsorption.

Freundlich equation is a purely empirical model, which is indicative of the surface heterogeneity of the sorbent, and is given by the following equation:

$$q_e = k_f c_e^{1/n_f} \tag{8}$$

where k_f is the Freundlich constant, $1/n_f$ is the heterogeneous coefficient, it is generally considered that substances with $1/n_f$ between 0.1 and 0.5 are easy to be adsorbed, and when $1/n_f > 2$, they are difficult to be adsorbed.

Temkin equation:

$$q_e = B \ln c_e + A \tag{9}$$

where B is Temkin's isothermal energy constant, and A is Temkin's isothermal energy constant.

Dubinin-Radushkevich isotherm model is used to describe sorption on both homogeneous and heterogeneous surfaces [39]. It can be expressed as follows:

$$q_e = q_D \exp\left\{-A_D\left[\text{In}\left(1 + \frac{1}{c_e}\right)\right]^2\right\} \tag{10}$$

where q_D is the adsorption capacity of adsorbent, mg•g^{-1}, and A_D is related to the free energy of adsorption.

The linear correlation coefficient shown in Table 6 indicates that the adsorption process is most consistent with the Langmuir equation, indicating that monolayer adsorption occurs on the surface of adsorbents. The $1/n_f$ in the Freundlich equation is less than 0.5, suggesting the favorable adsorption process [40].

The adsorption isotherms were analyzed by three-parameter models as follows:

Figure 16: The mechanism of chemisorption of boron chloride on adsorbents.

Redlich-Peterson equation:

$$q_e = \frac{A_{RP} C_e}{1 + B_{RP} c_e^g} \tag{11}$$

where A_{RP} and B_{RP} are the Redlich-Peterson constants;

Sips model:

$$q_e = \frac{q_s (K_s C_e)^{1/n_s}}{1 + (K_s C_e)^{1/n_s}} \tag{12}$$

where K_s is the adsorption equilibrium constant, and $q_s$is the adsorption capacity of adsorbent, mg•g^{-1};

Toth equation:

$$q_e = \frac{q_T K_t c_e}{\left[1 + (K_t c_e)^t\right]^{1/t}} \tag{13}$$

where K_t is the adsorption equilibrium constant, q_T is the adsorption capacity at equilibrium, mg•g^{-1}, $t = 1$, which proves that the adsorption process occurs on the monolayer adsorption surface.

The g of the Redlich-Peterson, n_s of Sips, and t of Toth models obtained in Table 7 are not equal to 1, indicating that the adsorption process occurs on the heterogeneous surface of multilayer adsorption, which is inconsistent with the analysis results of Langmuir isothermal adsorption model. The linear correlation coefficients are all less than 0.9, indicating that the three-parameter adsorption isothermal model is less suitable than the two-parameter model for the adsorption process of boron chloride on silicon oxide.

3.8. Chemisorption Mechanism. After completing adsorption, FT-IR spectra of adsorbents in Figure 15 show the appearance of new peak at 1400 cm^{-1} (as-B-O) [41], suggesting the chemisorption of boron chloride on the adsorbents.

Due to the significant electron deficiency of the boron, it can form typical covalent coordination bonds with electron donor, and the following mechanism of nucleophilic addition reactions is proposed in Figure 16 for the chemisorption of boron chloride on modified adsorbents.

The lone pair of electrons of polyhydric alcohols was coordinated to the electron deficient boron, and after accepting electrons, the Cl^- left with a pair of electrons, due to the strong polarity of the B-Cl bond, followed by the leaving of proton on the methanol. The total reaction is $3ROH + BCl_3 == B(OR)_3 + 3HCl$, similar to the hydrolysis of BCl_3 [42].

4. Conclusions

In this study, the silicon dioxide modified by oxygen–containing functional groups (–OH and –COO–) shows a better performance of the boron chloride removal in polysilicon production than that of chelating resign under the test conditions. The adsorption performance and adsorption mechanism of boron chloride are firstly discussed and described in detail, which are the relative lack in the previous industrial methods.

This study has given encouraging results, and organic-inorganic hybrid materials could be applied to reduce boron chloride. We wish to carry out the adsorption tests in the condition of flammable and explosive chlorosilane, which is closer to the industrial production, and this part has been left for future research.

Data Availability

The data used to support the findings of this study are available from the corresponding author upon request.

Conflicts of Interest

The authors declared no potential conflicts of interest with respect to the research, authorship, and/or publication of this article.

Acknowledgments

Our research was supported by Tianjin University and Zhejiang Shaoxing Institute of Tianjin University.

References

[1] P. Berberi, S. Thodhorjani, P. Hoxha, and V. Muda, "Photovoltaics: between a bright outlook and uncertainty," *Energy Science & Engineering*, vol. 1, no. 2, pp. 72–80, 2013.

[2] A. Allouhi, S. Rehman, M. S. Buker, and Z. Said, "Up-to-date literature review on solar PV systems: technology progress market status and R&D," *Journal of Cleaner Production*, vol. 362, article 132339, 2022.

[3] H. Chen, K. Morita, X. Ma, Z. Chen, and Y. Wang, "Boron removal for solar-grade silicon production by metallurgical route: a review," *Solar Energy Materials & Solar Cells*, vol. 203, article 110169, 2019.

[4] K. Yasuda, K. Morita, and T. H. Okabe, "Processes for production of solar-grade silicon using hydrogen reduction and/or thermal decomposition," *Energy Technol (Weinh)*, vol. 2, no. 2, pp. 141–154, 2014.

[5] China National Standards, "Solar-grade polycrystalline silicon," China National Standardization Management Committee, 2017, GB/T 25074-2017, 2017-11-01.

[6] China National Standards, "Electronic-grade polycrystalline silicon," China National Standardization Management Committee, 2014, GB/T 12963-2014, 2014-12-31.

[7] H. Qian and G. Huang, "Progress in the technology of high efficient removal of trace boron and phosphorus from trichlorosilane," *Chemical Industry and Engineering*, vol. 35, no. 2, pp. 42–48, 2018.

[8] H. Lu and X. Zhu, "Research development in the technology of boron removal from trichlorosilane," *Materials Review*, vol. 27, no. 5A, pp. 29–32, 2013.

[9] F. Li, H. Wang, L. Wang et al., "Processing crude trichlorosilane, by performing gas stripping treatment of crude trichlorosilane, and subjecting dichloro-dihydro-containing silicon and mixture of trichlorosilane and silicon tetrachloride to first purification treatment," 2015, 2015-139710, CN104261412-A; CN104261412-B.

[10] S. Chen, T. Lin, and H. Zhang, "Method of removing impurities in trichlorosilane mixed gas, involves spraying trichlorosilane mixed gas in gas-steam mixture wetting tower using silicon tetrachloride liquid and adsorbing silicon dust by silicon tetrachloride liquid," 2010, 2011-B02394, CN101913609-A.

[11] Z. Cao, W. Mao, W. Jiang, X. Sun, and Z. Jin, "Method of removing phosphorus-boron impurities from trichlorosilane, involves contacting trichlorosilane gas containing phosphorus-boron impurities with steam and inert gas, performing partial hydrolysis, distilling and purifying," 2010, 2011-B08030, CN101920961-A; CN101920961-B.

[12] Y. Guo, J. He, Z. Li, Q. Tang, and B. Zhao, "Removing boron and phosphorus during polysilicon production by modified Siemens process, comprises e.g. reacting silicon powder and hydrogen chloride to prepare synthetic trichlorosilane gas and reacting it with wet gas," 2010, 2011-B08030, CN101759186-A; CN101759186-B.

[13] E. H. R. Mueh, "Installation and method for reducing the content in elements, such as boron, of halosilanes," US Patent 2011052474(A1), 2011.

[14] W. E. Winter and R. Diaz, "Purification of halogenated silicon compounds," US Patent 3069239(A), 1962.

[15] J. Chen, P. Zhang, G. Xu, and H. Ke, "Method of absorbing parts per billion level boron and phosphorus impurities in trichlorosilane, comprises taking liquid, rectifying and purifying trichlorosilane, entering into each vaporizer, heating, passing into fixed bed and adsorbing," 2016, 2016-14255Y, CN105329902-A; CN105329902-B.

[16] S. Miyao, M. Ishida, and S. Nezu, "Purification of chlorosilane for silicon crystal growth involves circulating trichlorosilane which contains phosphorus trichloride and trichlorinated boron as impurity to anion exchange resin and disproportionating trichlorinated boron," 2015, 2015-70904R, JP2015202991-A; JP6184898-B2.

[17] F. Li, H. Wang, G. Yao, Y. Zhang, J. Bai, and S. Peng, "Purifying trichlorosilane involves cooling trichlorosilane, and then adsorbing cooled trichlorosilane in adsorption tower for adsorption of boron and phosphorus to get purified trichlorosilane," 2015, 2015-591862, CN104828827-A; CN104828827-B.

[18] L. Yang, T. Luo, Z. Xu, M. Shi, and Y. Min, "Boron-removing device in manufacturing trichlorosilane comprises a first and a second boron-removing tower, which are connected in series and communicated via rectifying tower and low styrene content resin filler layers in two towers," 2011, 2011-J90255, CN201890773-U.

[19] L. Wang, T. Qi, H. Li, and Y. Zhang, "Synthesis of a novel boron-specific chelating resin and its adsorption to boron from salt lake brine," *The Chinese Journal of Process Engineering*, vol. 4, no. 6, pp. 502–507, 2004.

[20] A. A. Oladipo and M. Gazi, "High boron removal by functionalized magnesium ferrite nanopowders," *Environmental Chemistry Letters*, vol. 14, no. 3, pp. 373–379, 2016.

[21] A. A. Oladipo and M. Gazi, "Hydroxyl-enhanced magnetic chitosan microbeads for boron adsorption: parameter optimization and selectivity in saline water," *Reactive and Functional Polymers*, vol. 109, pp. 23–32, 2016.

[22] A. A. Oladipo and M. Gazi, "Efficient boron abstraction using honeycomb-like porous magnetic hybrids: assessment of techno-economic recovery of boric acid," *Journal of Environmental Management*, vol. 183, pp. 917–924, 2016.

[23] L. T. Zhuravlev, "Concentration of hydroxyl groups on the surface of amorphous silicas," *Langmuir*, vol. 3, no. 3, pp. 316–318, 1987.

[24] S. Sugimura, K. Matsuoto, M. Kobayashi et al., "Purification of chlorosilane e.g. dichlorosilane used as raw material for preparing polycrystalline silicon, involves contacting crude chlorosilane containing boron compound with ion-exchange resin and silica adsorbenty2011-C09644, WO2011024276-A1.

[25] G. W. Sears, "Determination of specific surface area of colloidal silica by titration with sodium hydroxide," *Analytical Chemistry*, vol. 28, no. 12, pp. 1981–1983, 1956.

[26] J. S. Chen, H. M. Lin, and M. H. Yang, "Spectrophotometric determination of trace and ultratrace levels of boron in silicon and chlorosilane samples," *Fresenius' Journal of Analytical Chemistry*, vol. 340, no. 6, pp. 357–362, 1991.

[27] K. Joanna, C. Jerzy, T. Jolanta, Z. Maria, T. Marian, and D. Piotr, "Removal of boron dissolved in water," *Environmental Progress & Sustainable Energy*, vol. 26, no. 1, pp. 71–77, 2007.

[28] Z. C. Çelik, B. Z. Can, and M. M. Kocakerim, "Boron removal from aqueous solutions by activated carbon impregnated with

salicylic acid," *Journal of Hazardous Materials*, vol. 152, no. 1, pp. 415–422, 2008.

[29] A. A. Oladipo, E. O. Ahaka, and M. Gazi, "High adsorptive potential of calcined magnetic biochar derived from banana peels for Cu2+, Hg2+, and Zn2+ ions removal in single and ternary systems," *Environmental Science and Pollution Research International*, vol. 26, no. 31, pp. 31887–31899, 2019.

[30] H. Liu, X. Ye, Q. Li et al., "Boron adsorption using a new boron-selective hybrid gel and the commercial resin D564," *Colloids and Surfaces A: Physicochemical and Engineering Aspects*, vol. 341, no. 1-3, pp. 118–126, 2009.

[31] L. Wang, T. Qi, and Y. Zhang, "Novel organic-inorganic hybrid mesoporous materials for boron adsorption," *Colloids and Surfaces A: Physicochemical and Engineering Aspects*, vol. 275, no. 1-3, pp. 73–78, 2006.

[32] I. Sava, A. Burescu, and G. Lisa, "Study of thermal behavior of polyimides containing pendent-substituted azobenzene units," *Polymer Bulletin (Berlin)*, vol. 71, no. 6, pp. 1359–1373, 2014.

[33] X. Y. Liu and W. D. Yu, "Evaluating the thermal stability of high performance fibers by TGA," *Journal of Applied Polymer Science*, vol. 99, no. 3, pp. 937–944, 2006.

[34] E. S. Freeman and B. Carroll, "The application of thermoanalytical techniques to reaction kinetics: the thermogravimetric evaluation of the kinetics of the decomposition of calcium oxalate monohydrate," *The Journal of Physical Chemistry*, vol. 62, no. 4, pp. 394–397, 1958.

[35] W. Bouguerra, A. Mnif, B. Hamrouni, and M. Dhahbi, "Boron removal by adsorption onto activated alumina and by reverse osmosis," *Desalination*, vol. 223, no. 1-3, pp. 31–37, 2008.

[36] W. Bouguerra, I. Marzouk, and B. Hamrouni, "Equilibrium and kinetic studies of adsorption of boron on activated alumina," *Water environment research : a research publication of the Water Environment Federation*, vol. 81, no. 12, pp. 2455–2459, 2009.

[37] V. Russo, C. Rossano, E. Salucci, R. Tesser, T. Salmi, and M. Di Serio, "Intraparticle diffusion model to determine the intrinsic kinetics of ethyl levulinate synthesis promoted by Amberlyst-15," *Chemical Engineering Science*, vol. 228, p. 115974, 2020.

[38] D. Wei, B. Shuqin, M. Haorong, and N. Gaowa, "Investigation of phosphate removal from aqueous solution by both coal gangues," *Water Science and Technology: a Journal of the International Association on Water Pollution Research*, vol. 76, no. 4, pp. 785–792, 2017.

[39] Ö. Kaftan, M. Açıkel, A. E. Eroğlu, T. Shahwan, L. Artok, and C. Ni, "Synthesis, characterization and application of a novel sorbent, glucamine- modified MCM-41, for the removal/preconcentration of boron from waters," *Analytica Chimica Acta*, vol. 547, no. 1, pp. 31–41, 2005.

[40] H. Demey, J. Barron-Zambrano, T. Mhadhbi et al., "Boron removal from aqueous solutions by using a novel alginate-based sorbent: comparison with Al2O3 particles," *Polymers (Basel)*, vol. 11, no. 9, p. 1509, 2019.

[41] X. Zhang, X. Yu, Y. Chen, C. Zheng, and G. Zhao, "Synthesis of poly ethylene glycol boronic ester," *Fine Chemicals*, vol. 26, no. 7, pp. 652–655, 2009.

[42] N. R. Delue and J. C. Crano, "Boron tri:chloride prodn. by chlorinating borate ester - in presence of free radical initiator, reducing phosgene formation (NL 30.9.80)," 1980, 1980-71869C, DE3011246-A.